Pergamon

Geochimica et Cosmochimica Acta, Vol. 67, No. 2, pp. 197–211, 2003

0016-7037/03 $22.00 + .00

PII S0016-7037(02)01084-0

Orthoclase dissolution kinetics probed by in situ X-ray reflectivity: Effects of temperature, pH, and crystal orientation

P. FENTER,[1,*] C. PARK,[1] L. CHENG,[1] Z. ZHANG,[2] M. P. S. KREKELER,[3] and N. C. STURCHIO[1,3]

[1]Environmental Research Division, Argonne National Laboratory, Argonne, IL 60439, USA
[2]Dept. of Materials Science and Engineering, Northwestern Univ., Evanston IL 60208, USA
[3]Dept. of Earth and Environmental Sciences, Univ. of Illinois at Chicago, Chicago IL 60607, USA

(*Received November* 13, 2001; *accepted in revised form July* 27, 2002)

Abstract—Initial dissolution kinetics at orthoclase (001) and (010) cleavage surfaces were measured for ~2 to 7 monolayers as a function of temperature using in situ X-ray reflectivity. The sensitivity of X-ray reflectivity to probe mineral dissolution is discussed, including the applicability of this approach for different dissolution processes and the range of dissolution rates (~10^{-12} to 10^{-6} mol/m^2/sec) that can be measured. Measurements were performed at pH 12.9 for the (001) surface and at pH 1.1 for the (001) and (010) surfaces at temperatures between 46 and 83°C. Dissolution at pH 12.9 showed a temperature-invariant process with an apparent activation energy of 65 ± 7 kJ/mol for the (001) cleavage surface consistent with previous powder dissolution results. Dissolution at pH 1.1 of the (001) and (010) surfaces revealed a similar process for both surfaces, with apparent activation energies of 87 ± 7 and 41 ± 7 kJ/mol, respectively, but with systematic differences in the dissolution process as a function of temperature. Longer-term measurements (five monolayers) show that the initial rates reported here at acidic pH are greater than steady-state rates by a factor of 2. Apparent activation energies at acidic pH differ substantially from powder dissolution results for K-feldspar; the present results bracket the value derived from powder dissolution measurements. The difference in apparent activation energies for the (001) and (010) faces at pH 1.1 reveals an anisotropy in dissolution kinetics that depends strongly on temperature. Our results imply a projected ~25-fold change in the ratio of dissolution rates for the (001) and (010) surfaces between 25 and 90°C. The dissolution rate of the (001) surface is higher than that of the (010) surface above 51°C and is projected to be lower below this temperature. These results indicate clearly that the kinetics and energetics of orthoclase dissolution at acidic pH depend on crystal orientation. This dependence may reflect the different manifestation of the Al-Si ordering between the T1 and T2 tetrahedral sites at these two crystal faces and can be rationalized in terms of recent theoretical models of mineral dissolution.

1. INTRODUCTION

The chemical weathering of feldspars has been studied for many years using a variety of macroscopic (e.g., powder dissolution, surface charging) and microscopic (e.g., spectroscopic and imaging probe) approaches to gain insight into the associated microscopic processes, kinetics, and energetics. Feldspar dissolution is generally thought to proceed by a surface-controlled process involving disruption of the aluminosilicate network through elementary hydrolysis reactions. Laboratory measurements (e.g., Petroviç, 1976; Chou and Wollast, 1984; Holdren and Speyer, 1985; Casey et al., 1989; Muir et al., 1989; Schweda, 1989; Inskeep et al., 1991; Stillings and Brantley, 1995; Hellmann, 1995; Hellmann et al., 1997; Gout et al., 1997; Nugent et al., 1998; Jordan et al., 1999; Chen et al., 2000) suggest that the mechanisms of feldspar-water interfacial reactions may be distinctly different under acidic and alkaline conditions, based on the thickness of leached surface layers, the pH dependence of dissolution kinetics, and the apparent activation energies measured in each pH regime (Blum and Stillings, 1995). This implies that the rate-limiting reactions are different in these two regimes and that the individual reactions can be isolated at extreme values of pH. Observations by numerous workers indicate that dissolution is nonstoichiometric at acidic pH over a broad range of temperatures (Petrovich, 1976; Chou and Wollast, 1984; Holdren and Speyer, 1985; Casey et al., 1989; Muir et al., 1989; Hellmann et al., 1990, 1997; Inskeep et al., 1991; Stillings and Brantley, 1995; Nugent et al., 1998; Chen et al., 2000) and nearly stoichiometric at alkaline pH near room temperature (Holdren and Speyer, 1985; Casey et al., 1989; Hellmann et al., 1997), although nonstoichiometric dissolution has also been observed at alkaline pH at elevated temperatures (Hellmann et al., 1990; Hellmann, 1995). A substantial body of theoretical work has been developed to relate these macroscopic observations to the associated microscopic processes. Most of this work has used the analogy with simpler mineral systems in which the dissolution rate is related to protonation/deprotonation reactions that occur at the surface (Walther, 1997; Brantley and Stillings, 1997). Quantum mechanical calculations of idealized aluminosilicate clusters have been performed to test the relative proton affinities of different bonds (Kubicki et al., 1996).

In many cases, measurements of feldspar powder dissolution rates as a function of temperature have been analyzed to derive

* Author to whom correspondence should be addressed (fenter@anl.gov).

apparent activation energies through Arrhenius behavior (Blum and Stillings, 1995, and references therein; Chen and Brantley, 1997). However, the extent to which powder dissolution results represent individual molecular-scale processes or an ensemble average of different processes (e.g., due to the distribution of surface orientations, morphologies, etc., associated with powder measurements) has yet to be thoroughly explored. To our knowledge, few measurements have explored the anisotropy of feldspar dissolution. In one measurement, the anisotropy of dissolution rates was measured using batch solution chemical analyses at acidic pH and $T > 90°C$ using thin labradorite disks polished along the three principle crystallographic directions, but they did not reveal any systematic anisotropy of the dissolution rate or activation energies (Suzuki et al., 1996). Recent dissolution measurements of fosteritic olivine demonstrated a ~40% variation in apparent activation energy for three crystallographic orientations (Awad et al., 2000).

A more fundamental understanding of mineral dissolution can be obtained by probing dissolution at the molecular scale. Since the seminal work of Gratz et al., (1990, 1991), in which the dissolution rates of quartz surfaces were estimated using ex situ atomic force microscopy (AFM) and optical microscopy, there have been numerous in situ measurements of step and kink motion on well-characterized surfaces that provide a fundamental basis for determining overall mineral dissolution rates (e.g., Hillner et al., 1992; Bosbach and Rammensee, 1994; Liang et al., 1996; Liang and Baer, 1997; Jordan and Rammensee, 1998; Shiraki et al., 2000). This approach has been successful, but its application can be limited by a number of factors. First, measurements of dissolution rates are usually derived from the velocity of individual steps and consequently the mineral of interest must dissolve primarily by step motion. Second, many minerals cannot be studied using in situ AFM, because the dissolution rates must be compatible with AFM scanning rates (Dove and Platt, 1996). The advent of the hydrothermal AFM (Higgins et al., 1998; Jordan et al., 1999) has extended the range of minerals that can be studied by this approach by increasing the dissolution rates of less reactive minerals. Such molecular scale measurements of dissolution are therefore likely to provide new insight into some of the widely observed characteristics of feldspar dissolution, including non-stoichiometry of dissolution and the initially fast transient dissolution kinetics.

One promise of molecular-scale approaches to mineral dissolution is to determine the extent to which either the dissolution rates or processes depend on the crystal faces of a mineral. Face-selected dissolution rates and their associated activation energy have been determined for the prismatic and rhombohedral faces of natural quartz growth surfaces with AFM, and little anisotropy was found in the dissolution rates or activation energies (Gratz et al., 1990). The reported activation energies were in agreement with powder dissolution studies (Dove, 1995).

We have previously demonstrated the ability to probe the structure and dissolution processes of the orthoclase (001)-fluid interface using X-ray reflectivity and atomic force microscopy (Fenter et al., 2000; Teng et al., 2001). These results are briefly reviewed since they provide a conceptual foundation to the present results and highlight the sensitivity of X-ray reflectivity to probe mineral dissolution processes. Specular X-ray reflectivity measurements revealed the molecular-scale structure and termination of the orthoclase (001)-water interface in deionized water, including observations that only the outermost potassium ions are removed after brief contact with de-ionized water; the surface tetrahedral sites are fully hydroxylated; and the surface tetrahedral sites are displaced by ~0.15 Å with respect to the bulk structure with significant relaxations observed as deep as ~26 Å into the crystal (Fenter et al., 2000). In situ measurements of the dissolution of orthoclase (001) surfaces at extreme pH provided new insight into the dissolution processes (Teng et al., 2001). These results demonstrated that dissolution follows a layer-by-layer process at both acidic and alkaline pH, as evidenced by an oscillatory change in the X-ray reflectivity as a function of time during dissolution. Each oscillation of the reflectivity corresponds to the removal of a single layer of orthoclase. This layer-by-layer character of the dissolution process implies that there are two reactive sites in each pH regime associated with terrace- and step-specific processes. The dominant process at alkaline pH is a step-specific process, whereas step- and terrace-specific processes have comparable rates at acidic pH; that is, the spatial distribution of reactive sites changes significantly with pH. These results provide new insight into the transient dissolution kinetics widely observed in powder dissolution measurements; no clear evidence was found for significant variation of the dissolution kinetics during dissolution of freshly cleaved surfaces, especially with respect to the $>10\times$ variation observed in powder dissolution measurements. However, a substantial transient dissolution rate was observed after switching from acidic to alkaline solutions. This phenomenon was explained by the different reactivity of step and terrace sites in the two pH regimes: (1) The proliferation of steps during dissolution at acidic pH provided extensive step densities and (2) the high reactivity of such sites at alkaline pH resulted in a rapid but brief transient dissolution period, after which the intrinsic dissolution rate at this temperature was again observed. We also found, through high-resolution X-ray reflectivity measurements of reacted surfaces, that the dissolution process was fully stoichiometric at alkaline pH with no significant change in the orthoclase surface after dissolution. Similar measurements at acidic pH revealed that dissolution was minimally non-stoichiometric (non-stoichiometric depths of < 6.5 Å were observed after dissolution of ~25 layers).

In this paper we extend these previous results to show that X-ray reflectivity (Feidenhans'l, 1989; Robinson and Tweet, 1992) can be used to determine precise crystal face-specific dissolution rates and their variation with temperature at pH 1.1 and 12.9. We also discuss the accuracy of these results by comparison with powder dissolution measurements and through measurements performed over longer time periods. These are the first in situ molecular-scale measurements of face-specific activation energies of feldspar dissolution. New measurements were performed on the orthoclase(001) surface at pH 1.1 and 12.9 to isolate the individual pH-dependent dissolution processes (as identified by Teng et al., 2001). The anisotropy of the dissolution process is also explored at pH 1.1 by comparing the dissolution rates of the structurally similar (001) and (010) cleavage surfaces. We demonstrate that the apparent activation energies for dissolution of particular surfaces can differ substantially from each other and from those obtained from powder dissolution measurements. This indi-

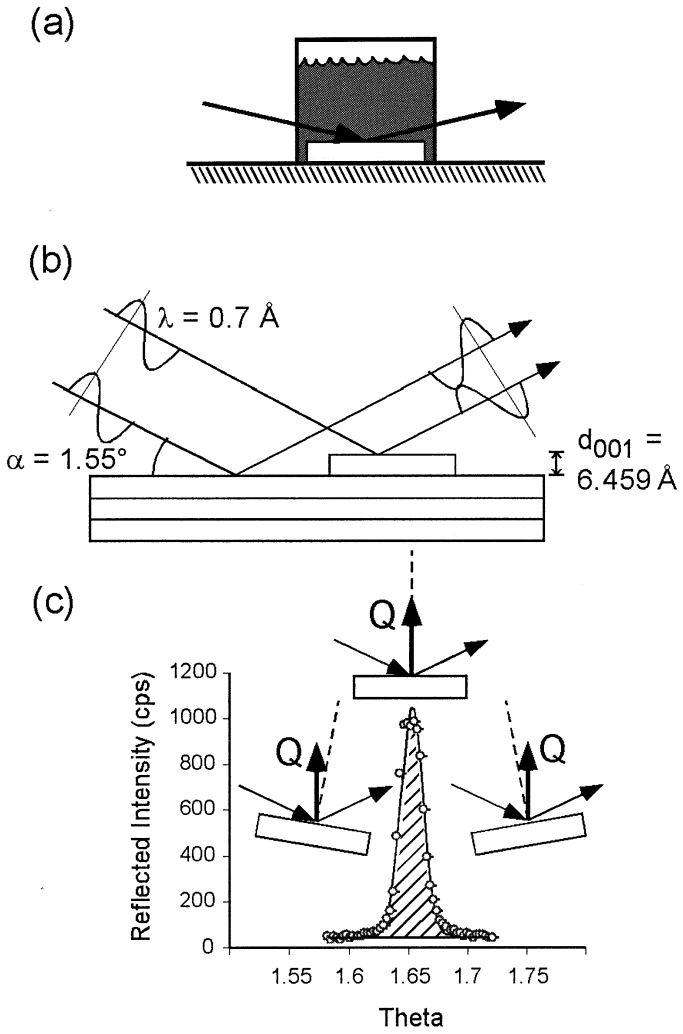

Fig. 1. (a) Schematic diagram of the transmission sample cell. (b) Schematic diagram of the interference of X-rays reflected from neighboring terraces at the "anti-Bragg" condition. (c) A rocking curve at n = 1/2 for a freshly cleaved orthoclase surface. The hashed area is proportional to the integrated reflectivity. Insets in (c) schematically show the orientation of the sample at three points of the rocking curve, as well as the incident and reflected X-ray beams, the momentum transfer (bold arrow), and the specular reflectivity rod (dashed line). The specular reflection condition is satisfied when the momentum transfer vector coincides with the specular reflectivity rod.

cates that apparent activation energies derived from powder dissolution measurements are not generally representative of individual molecular-scale processes, but instead reflect the average response of a potentially complex distribution of cleavage faces and fracture surfaces. The theory of Casey and Sposito (1992) is used to provide a possible explanation for an understanding of this kinetic anisotropy and, in particular, the correlation of apparent activation energies with aluminol site densities on these two surfaces.

2. EXPERIMENTAL DETAILS

We examined the evolution of dissolving orthoclase (001) and (010) cleavage surfaces using gem-quality homogeneous crystals (Itrongay, Madagascar; Kimata et al., 1996). Electron microprobe analyses yielded a chemical formula, based on eight oxygens, of $K_{0.96}Na_{0.04}Al_{0.96}Fe_{0.04}Si_{3.00}O_{8.00}$ (Fenter et al., 2000). Examination of this material using back-scattered electron imaging, transmission electron microscopy, cathodoluminescence, and transmitted light optical microscopy revealed no evidence of albite exsolution lamellae or other microstructures. Based on the crystallographic parameters at 296 K, a = 8.574 Å, b = 13.006 Å, c = 7.191 Å, $\alpha = 90°$, $\beta = 116.07°$, $\gamma = 90°$ with C2/m symmetry (Kimata et al., 1996), the vertical separations between the (001) and (020) Bragg planes are, respectively, $d_{001} = c \times \sin(\beta) = 6.459$ Å and $d_{020} = b/2 = 6.503$ Å (Kimata et al., 1996).

X-ray reflectivity data were collected in situ at 46 to 83°C in flowing solutions of 0.1-mol/L HCl and 0.1-mol/L NaOH having pH values (at 25°C) of 1.1 and 12.9, respectively. Time-resolved measurements of dissolution kinetics and processes were performed in a flow-through Teflon sample cell in transmission geometry with a ~3.5-mm path-length of X-rays through water and two 0.13-mm Kapton windows (Fig. 1a). The sample cell volume was 1.0 mL. The footprint of the X-ray

beam was adjusted to be ~10% smaller than the sample length (~3.5 mm) along the beam direction and ~1-mm transverse to the beam direction. Surfaces examined by X-ray reflectivity were prepared by cleavage of orthoclase crystals along the (001) or (010) planes; orthoclase has perfect cleavage in these two directions. Each sample was loaded into the X-ray cell with 1-mL deionized water immediately (within 1 min) after cleavage, and sample alignment in the X-ray beam was performed at 25°C. The cell was then externally heated to the desired temperature, taking advantage of the ~1000× slower dissolution rate at pH 6 as compared with pH 1 and 13 (e.g., Blum and Stillings, 1995, and references therein). To change the pH, we rapidly displaced the deionized water from the cell with ~10 mL of solution resulting in a brief (~2 min) decrease of the fluid temperature that was monitored continuously by a thermocouple positioned in the solution ~2 mm above the sample surface. We then continued to supply fresh solution to the cell throughout the experiment using a syringe pump at 3-mL h^{-1}.

Synchrotron X-ray reflectivity measurements were made at the Advanced Photon Source (beamlines 12-ID, 11-ID, and 12-BM) using monochromatic X-rays ($\Delta E/E = 10^{-4}$). Photon energies ranging from 17.5 to 19.6 keV were used for different experiments but were not varied within a given experiment. The X-ray reflectivity is defined as the ratio of the reflected-to-incident flux. With high-brilliance synchrotron sources, reflectivities can be measured to $< 10^{-10}$, although the lower limit of sensitivity is affected by the level of diffuse X-ray background in the experimental configuration (e.g., caused by scattering from the solution, the X-ray window, and air in the beam path) and the amount of counting time needed to distinguish the reflectivity from the diffuse background.

3. RESULTS

3.1. Real-Time Measurements of Dissolution Using X-ray Reflectivity

Surface dissolution processes can be characterized by time-resolved measurements of X-ray reflectivity at the "anti-Bragg" condition. The angle of incidence, α, with respect to the surface plane is specified by Bragg's law, $n\lambda = 2d_{hkl}\sin(\alpha)$, where $n = 1/2$ for the first anti-Bragg condition, λ is the X-ray wavelength, and d_{hkl} is the Bragg plane spacing of the (hkl) planes. This scattering condition gives high sensitivity to changes in the mineral surface (e.g., morphology, structure, termination, composition) and maximizes sensitivity to interfacial roughness (Robinson, 1986). This sensitivity comes from destructive interference between X-rays that are reflected from neighboring terraces that differ in height by a single layer spacing (e.g., $d_{001} = 6.459$ Å for the (001) surface), as shown in Figure 1b. The destructive interference at $n = 1/2$ results in a strong variation of the reflectivity as a function of the occupation of this layer. The reflectivity is maximized when the outermost orthoclase layer is fully occupied and minimized when the outermost layer is approximately half occupied. In contrast, the X-rays reflected from neighboring terraces constructively interfere at scattering conditions specified by $n =$ integer corresponding to the Bragg condition; near this condition the reflectivity data are insensitive to changes in surface termination and instead are sensitive to the bulk crystal structure.

A typical "rocking scan" at the first anti-Bragg condition for a freshly cleaved orthoclase (001) surface, where the angular position of the detector was fixed while the incident angle, α, was taken through the specular reflection condition (Fig. 1c). The reflectivity at this scattering condition is $\sim 10^{-6}$ (Fenter et al., 2000). The reflectivity signal is clearly observed as a sharp peak having a width of ~0.02° that is superimposed on a flat background associated with incoherent scattering (e.g., from the solution). The rocking-curve width was equal to the experimental resolution as determined by half the angular detector slit size in the scattering plane (~0.04°), implying that the average surface domain size was larger than our lateral X-ray coherence length (~2 μm), which is consistent with previous AFM results (Teng et al., 2001). The integrated reflected flux and its associated uncertainty for each rocking curve are determined by least-squares fitting (Bevington, 1969). More details about our reflectivity measurement procedures are given elsewhere (Fenter et al., 2000; Teng et al., 2001).

In situ synchrotron X-ray reflectivity measurements of an orthoclase (001) cleavage surface as a function of time during dissolution at 73°C and pH 12.9 are shown in Figure 2a,b. The reflectivity was measured at regular time intervals. The shape of the rocking curve at the anti-Bragg condition ($n = 1/2$) did not change during dissolution (Fig. 2a). The specular reflectivity at $n = 1/2$, however, changed substantially and non-monotonically as dissolution progressed. The integrated reflectivity at the anti-Bragg condition ($n = 1/2$) as a function of time is shown in Figure 2b. The reflectivity shows a significant oscillatory variation with a slow decrease in the overall intensity at subsequent intensity maxima. Separate data taken during the same dissolution experiment at a scattering condition close to the orthoclase (002) Bragg condition show no systematic variation as a function of time in excess of statistical error (Fig. 2b). (Here, we perform the measurements at $n = 1.97$ instead of $n = 2$, because the intensity of the bulk Bragg peak exactly at $n = 2$ is too high to be measured by our detector. The interference phenomenon that is responsible for the sensitivity to dissolution is negligibly different between $n = 1.97$ and 2.) These invariant data at $n = 1.97$ are primarily sensitive to the bulk crystalline structure and insensitive to the surface structure and termination and prove that the variations observed in Figure 2a,b near $n = 1/2$ are exclusively due to changes in the near-surface region during dissolution and are not an artifact of the measurement process.

We have previously described how real-time X-ray reflectivity measurements provide insight into orthoclase dissolution processes (Teng et al., 2001). Specifically, the oscillations in the reflectivity vs. time can be associated with the successive removal of individual layers at the orthoclase surface (van der Vegt et al., 1992). It is important to emphasize that these measurements probe essentially the same quantity that is derived from a powder dissolution measurement (i.e., the net amount of material released to solution as a function of time), although X-ray reflectivity measures this quantity for a single cleavage surface. The data in Figure 2b show that the removal of successive layers (noted as "ML" for monolayer in the figure) at pH 12.9 occur every ~2.8 h at 73°C. The corresponding dissolution rate (in units of mole feldspar/m^2/s) can be calculated as $6 \times 10^{-6}/t_{ML}$ (where t_{ML} is the time in seconds to dissolve a single monolayer), corresponding to a net disso-

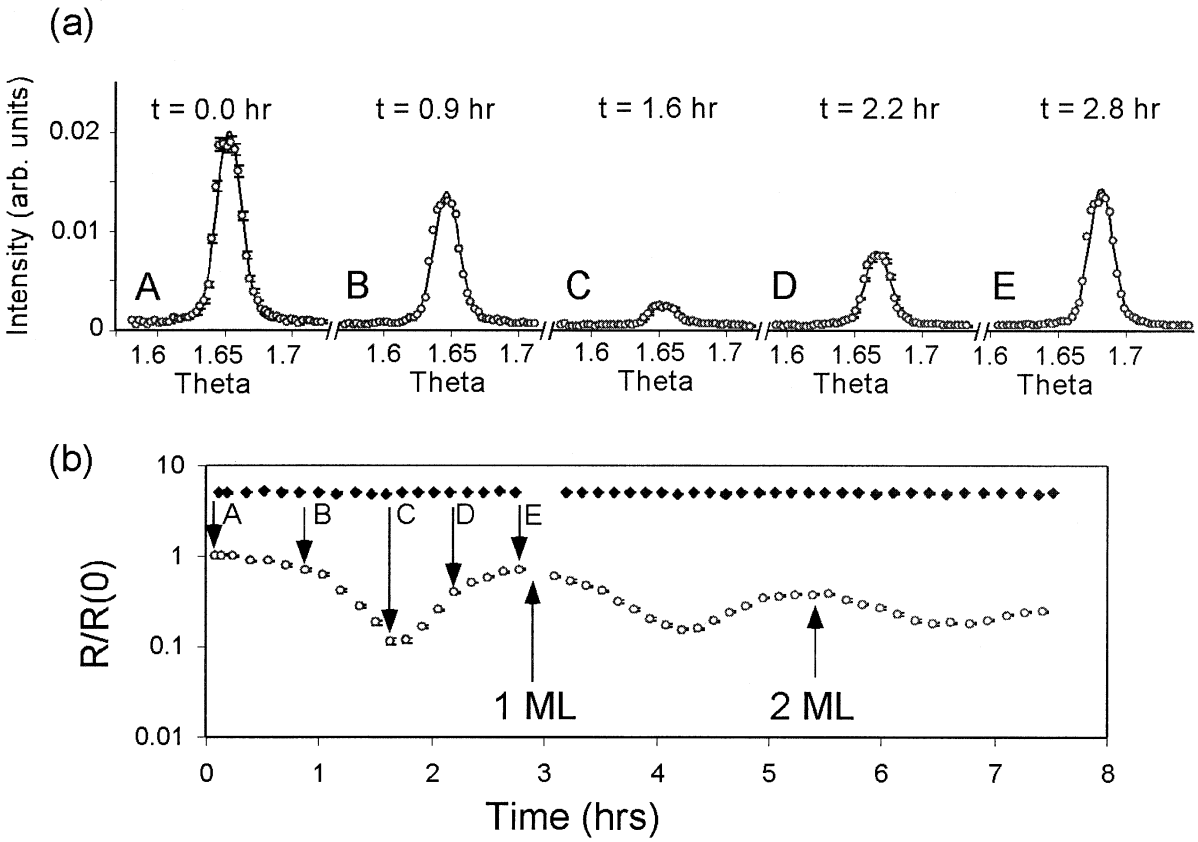

Fig. 2. (a) Rocking curves measured as a function of time at 73°C and pH 12.9. The peak shape does not change, but the integrated intensity of the peak changes substantially and non-monotonically as dissolution proceeds. (b) Integrated reflectivity as a function of time measured at n = 1/2 (open circles) and n = 1.97 (filled diamonds). The vertical axis for both sets of data is normalized to the initial value before exposure to the pH 12.9 solution, but the data at n = 1.97 are further offset by a factor of 5 for clarity. The reflectivities for the individual rocking scans in (a) are labeled for direct comparison. Each oscillation at n = 1/2 is associated with the removal of an individual orthoclase layer (noted as "ML"), while the reflectivity at n = 1.97 shows no significant change as a function of time.

lution rate of 6×10^{-10} mol/m^2/s (a single unit cell of orthoclase(001) corresponds to four $KAlSi_3O_8$ units/111.5 Å^2).

Changes in X-ray reflectivity with dissolution are large with respect to both the background and the statistical error in the measurement (derived from counting statistics). Because the data are also sensitive to interfacial termination, structure, and roughness, any change in such quantities as a function of time will be associated with an overall change of the reflectivity at successive reflectivity maxima. We determined previously that the termination and surface composition of orthoclase do not change significantly as a function of time at alkaline pH and that the overall decrease in reflectivity of successive reflectivity maxima is associated with a slow increase in the interfacial roughness during dissolution (Teng et al., 2001).

3.2. Dissolution Kinetics of Orthoclase (001) at pH 12.9

A series of real-time reflectivity measurements during dissolution of the orthoclase (001) surface for different temperatures at pH 12.9 is shown in Figure 3a. These data have similar slightly damped oscillatory reflectivity patterns over the temperature range studied (50−83.3°C), although the time between subsequent reflectivity maxima varies strongly with temperature. The dissolution rate is most simply estimated by noting the times at the first reflectivity maxima, t_{ML}. Based on this simple assessment, the results in Figure 3a confirm that there is a substantial change in the dissolution rate as a function of temperature at pH 12.9. This approach, however, has some inherent limitations. The first is that the time corresponding to the first reflectivity maximum may not be straightforward to determine if the reflectivity decreases strongly between reflectivity maxima (this is the case for dissolution at acidic pH). The second is that individual datasets may be incomplete (e.g., at or near the reflectivity maxima). Finally, the dissolution process might exhibit transient dissolution kinetics, whereby the dissolution rate depends on the amount of material dissolved.

A more general approach to determine the relative dissolution rates is to scale the time axis of each dataset by a factor $\tau(T)$. For a dissolution process that is invariant with respect to temperature (except for changes in the dissolution rate), the scaled reflectivity data, $R[t/\tau(T)]/R(t = 0)$, should be independent of the temperature. The magnitude of $\tau(T)$ can, in principle, be chosen arbitrarily for a single reference dataset, and in

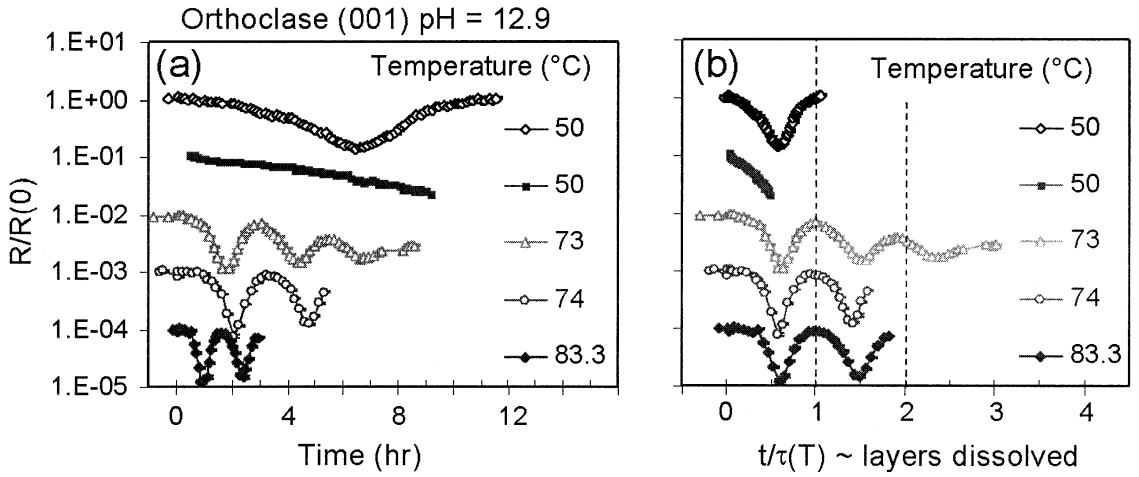

Fig. 3. In situ X-ray reflectivity measurements of dissolving orthoclase (001) surfaces at pH 12.9 and $50 \leq T \leq 83.3$°C, with each dataset vertically offset by factors of 10 for clarity. (a) Reflectivity vs. time and (b) the same data in which the time axis has been scaled by τ(T) to correspond to the number of dissolved layers.

this case, the variation of τ(T) with temperature will reflect only the relative changes in dissolution rates with respect to the reference data. We can, however, use our understanding of the dissolution process (specifically, the observation that each oscillation corresponds to the removal of a single layer of material) to obtain absolute dissolution rates by assigning τ(T) to be the time to remove a single layer at a temperature T. In this way, the scaled reflectivity data $R[t/\tau(T)]/R(t = 0)$ will oscillate with unit period, and the horizontal axis is transformed into a measure of the number of layers dissolved at the (001) surface (Fig. 3b). This is indicated by the location of subsequent maxima corresponding to integer values of $t/\tau(T)$, providing a simple and direct measure of the absolute dissolution rate. Precise values of the relative dissolution rates are determined by choosing values of τ at each temperature that optimize the visual agreement (i.e., "by eye") between different datasets. No one feature was used to determine τ for a particular dataset. In cases where there may appear to be a conflict between different aspects of the data (e.g., the location of subsequent maxima or the initial decrease of the reflectivity), the overall agreement between datasets was used as the primary criterion. The resulting scaled data are shown in Figure 3b. They show a nearly identical temperature-independent variation of the reflectivity as a function of scaled time, $t/\tau(T)$, for all the datasets. This indicates that there are no significant changes in the dissolution process over the measured temperature range. The dissolution rate corresponds to $1/\tau$, and the systematic variation of dissolution rate with temperature is discussed in detail below. This approach of scaling the time axis to determine the dissolution rates allows us to determine dissolution kinetics with partial datasets (an extreme example is the second dataset at 50°C in Fig. 3, during which a net dissolution of ~1/2 layer was measured).

3.3. Dissolution Kinetics at pH 1.1

3.3.1. Orthoclase (001)

Real-time reflectivity data taken at pH 1.1 between 50 and 76°C are shown in Figure 4a,b. As we reported previously (Teng et al., 2001), the data at acidic pH reflect a more random process in which the surface roughness increases substantially with increasing dissolution. This results in a substantial (~10-fold) decrease of the X-ray reflectivity at the first intensity maximum (Fig. 4a), with the reflectivity decreasing by as much as a factor of $\sim 10^3$ with respect to the initial value. This strong decrease in the reflectivity during dissolution makes it difficult to determine the dissolution rate simply from the location of subsequent maxima, since the precise locations of individual maxima can be altered by the strong decrease in overall intensity. Instead, the relative dissolution rates as a function of temperature were determined by normalizing the time axis (Fig. 4b), as described above.

There is greater variability in the time-normalized acidic dissolution data as compared with the alkaline dissolution data. For example, we observe a ~20% variation in the location of the second intensity maximum with respect to the predicted value of two layers in the time-normalized data (Fig. 4b). If we assume that this variability is due to experimental factors such as variability of surface quality, this provides an internal measure of the error in the overall dissolution rates. We also find that sample-to-sample variations in the shape of reflectivity vs. time data are also significant. For example, the intensity varies by factors of 5 at the first intensity minimum (at ~0.5 layers dissolved) and by as much as a factor of 15 at the second intensity minimum (at ~1.5 layers dissolved). However, variations in the shape of the data in Figure 4b imply that the interfacial structure is not strictly invariant after a given amount of dissolution (e.g., after 1/2 layer dissolved), implying that there are differences in the acidic dissolution process for these different samples. (A full structural determination at a given point during dissolution can be performed only when the variation of the reflectivity as a function of incident angle is measured over a broad range of angles.) From previous studies, we know that the acidic dissolution process is complex and includes substantial surface roughening, terrace etching, development of a thin (< 6.5-Å thick) nonstoichiometric layer, as well as the buildup of a gel-like layer at the surface under slow flow conditions (Teng et al., 2001). The variability in the data

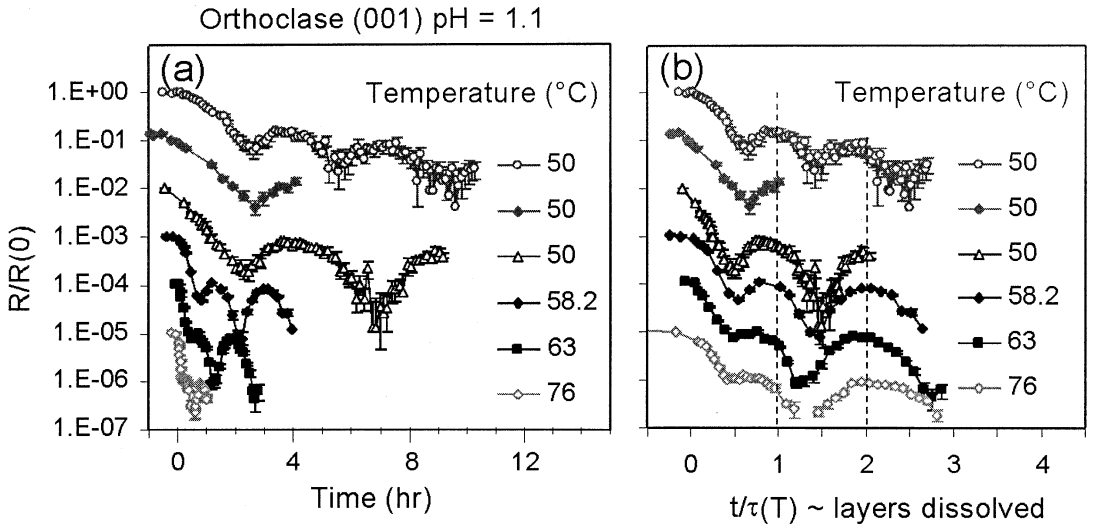

Fig. 4. In situ X-ray reflectivity measurements of dissolving orthoclase (001) surfaces at pH 1.1 and $50 \leq T \leq 76$°C, with each dataset vertically offset by factors of 10 for clarity. (a) Reflectivity vs. time and (b) the same data in which the time axis has been scaled to correspond to the number of dissolved layers.

in Figure 4b does not correlate with the time that the cleavage surface was in contact with water (ranging from 0.5–4.2 h) before the acid solution was introduced. The behavior is, however, weakly correlated with the sample temperature; the first intensity minimum (near ~0.5 layers dissolved) is smallest at lower temperatures and largest at the highest temperatures. This suggests that at least part of this variability is intrinsic to the acidic dissolution process and might be associated with the variation of potassium or aluminum depletion depths with temperature.

3.3.2. Orthoclase (010)

We have explored the crystallographic dependence of the dissolution kinetics through measurements of the orthoclase (010) surface. In comparing the (001) and (010) surfaces, we maintain the composition and structure of the mineral and change only the orientation of the cleavage plane with respect to the tetrahedral rings. As can be seen in Figure 5, the (010) surface is similar to the (001) surface in both the type and distribution of tetrahedral sites (both non-bridging and bridging oxygen sites), and its area per tetrahedral ring differs by only 0.6% from the (001) surface. As in the case of the (001) surface, we find resolution-limited rocking curves having widths of $< 0.04°$ indicative of large flat (010) terrace areas $>$ 2-μm wide.

Real-time dissolution data for the (010) surface at pH 1.1 are shown in Figure 6a. These data have the same strongly damped oscillatory behavior as that found for the (001) surface in which subsequent reflectivity maxima have decreasing intensities. This implies that the character of the dissolution process for the (010) surface is similar to that of the (001) surface. After normalizing the time axis (Fig. 6b), we find that the data superimpose in a way that is similar to that of the (001) surface at acidic pH and, again, with a higher degree of variability than was observed for the (001) surface at alkaline pH.

3.4. Transient Dissolution Kinetics

Before discussing the trends in dissolution rates measured above, it is useful to first make a comparison of the single-crystal and powder dissolution processes. Powder dissolution measurements at acidic pH are complicated by transient kinetics in which the initial dissolution rate is typically $> 10\times$ higher than the steady-state value, and it may take many hours or even days to reach a quasi-steady-state dissolution rate (Blum and Stillings, 1995; Chen and Brantley, 1997). There-

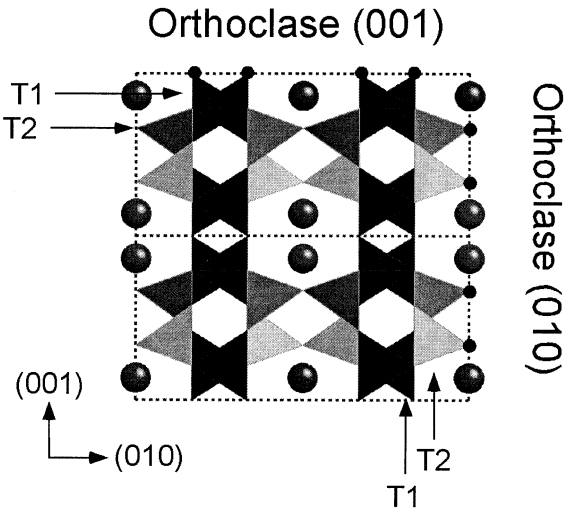

Fig. 5. Schematic diagram of the (001) and (010) cleavage surfaces. Also labeled are the two distinct tetrahedral sites in the orthoclase lattice (T1 and T2). The Al occupations are 0.352 and 0.148 for the T1 and T2 sites, respectively (Kimata et al., 1996). The T1 site expresses an NBO on the (001) surface, and the T2 site expresses an NBO on the (010) surface. (NBOs are indicated as small filled circles on the interfacial tetrahedral sites.)

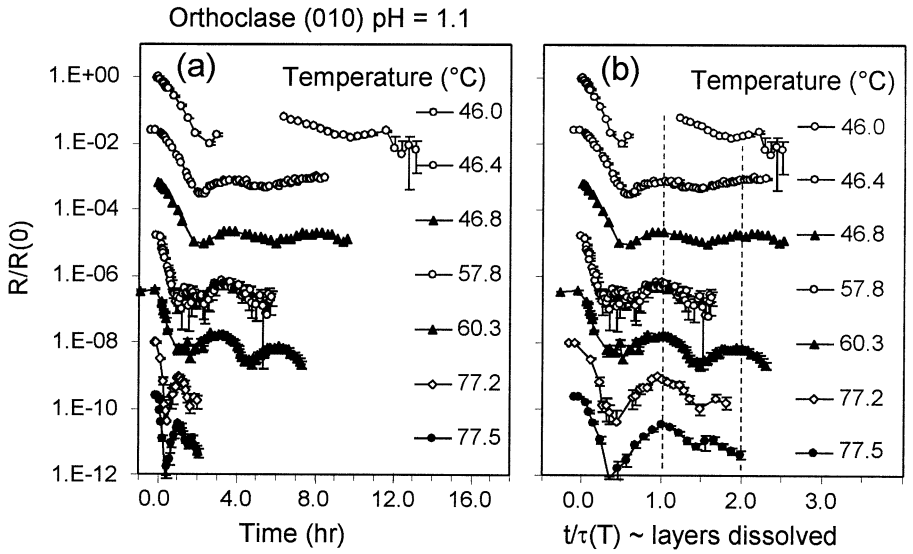

Fig. 6. In situ X-ray reflectivity measurements of dissolving orthoclase (010) surfaces at pH 1.1 and $46 \leq T \leq 77.5$°C, with each dataset vertically offset by factors of 40 for clarity. (a) Reflectivity vs. time at pH 1.1 and (b) the same data in which the time axis has been normalized to the number of dissolved layers.

fore, we must determine whether the present single-crystal results also show transient dissolution kinetics, and if so, the degree to which it affects the present results. Powder dissolution data are typically reported as amount of material dissolved as a function of time from a sample with a very high surface area. To compare with the X-ray reflectivity data, we must convert the amount dissolved to the number of equivalent dissolved monolayers. It is interesting to note that powder dissolution data for both microcline and albite (at acidic pH and $T \leq 100$°C) show that the net amount dissolved during the extreme non-steady-state period is approximately one monolayer of material (Schweda, 1989; Hellmann, 1994). After this period of time, the dissolution rate approaches a quasi-steady-state value, although results in the literature show that true steady-state results are achieved only after substantially longer time periods (Chen and Brantley, 1997).

To assess the degree to which the present single-crystal data are affected by these transient dissolution kinetics, we show in Figure 7 longer-term dissolution data for the (001) surface at pH 1.1 and T at 77°C. To highlight each oscillation in the reflectivity, we show vertical dashed lines corresponding to each reflectivity maximum. In Figure 8, we plot the layer-resolved dissolution rate as a function of the number of layers dissolved. These data clearly show that there is, indeed, a transient nature to the dissolution rates for the single cleavage surfaces, as measured by the oscillation period as a function of time. The initial dissolution rate is found to be essentially constant for dissolution of the first two layers. After this initial period, the dissolution rate appears to decrease by 50% and remains unchanged through dissolution of layers three through seven. This implies that the more extreme ($> 10\times$ faster) non-steady-state dissolution kinetics observed with powdered samples is not an intrinsic characteristic of the dissolution of orthoclase single crystals. Instead, the dissolution rates measured for freshly cleaved surfaces show at most a twofold change in dissolution kinetics. Furthermore, no significant transient dissolution kinetics have been observed at alkaline pH, although due to the slower dissolution kinetics at those condi-

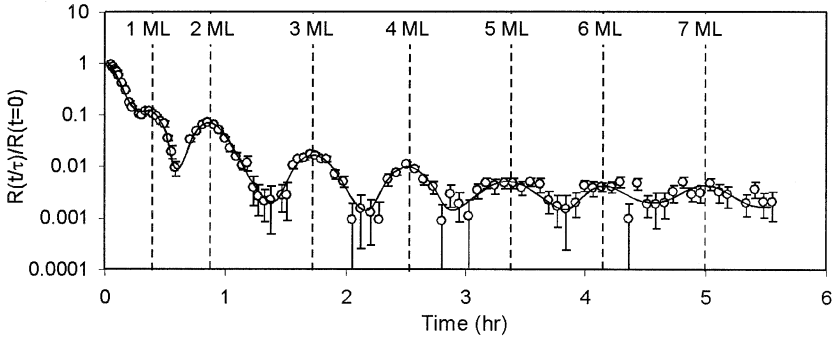

Fig. 7. Extended X-ray reflectivity measurements of dissolving orthoclase (001) surfaces at pH 1.1 and T at 77°C. The vertical dashed lines indicate the removal of the first to seventh monolayers. The solid line through the points is a guide to the eye.

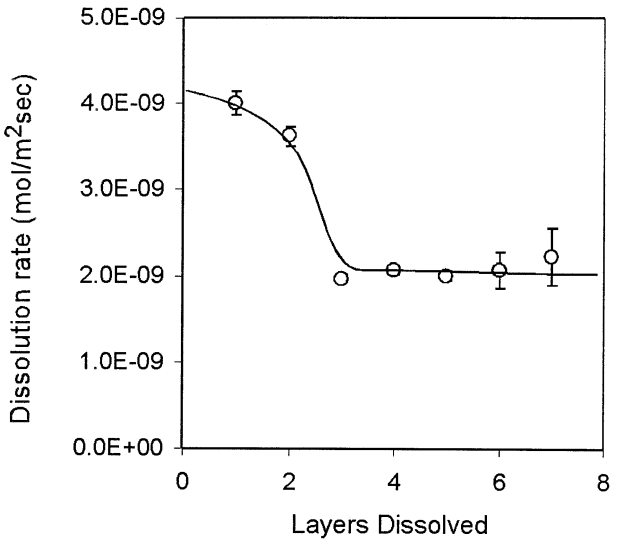

Fig. 8. Plot of the dissolution rate as a function of the number of dissolved layers at pH 1.1 and T at 77°C, derived from the data in Fig. 7. A steady-state dissolution rate is achieved upon dissolution of the third layer of orthoclase. The line is a guide to the eye.

tions, we have not observed dissolution kinetics beyond 3 ML for any given sample. Together, these observations suggest that we can directly compare the dissolution kinetics derived from X-ray reflectivity measurements to those from steady-state powder dissolution studies, especially given the ~10-fold variation found between individual powder dissolution studies (e.g., Blum and Stillings, 1995, and references therein).

In the context of these observations, we stress that our determination of the dissolution kinetics through the scaling the time-axis of the data emphasizes the *relative* dissolution rates that are derived from an analysis of the temperature-dependent scale factor, $\tau(T)$. In this sense, the uncertainty in the absolute dissolution rate due to transient kinetics is less important than the relative changes in dissolution rate that we can measure more precisely and from which we derive the apparent activation energies. Therefore, we expect that the apparent activation energies that we derive should be minimally affected by the relatively small transient nature of the dissolution kinetics at acidic pH.

3.5. Variation of the Dissolution Rate vs. Temperature

The systematic variation of the dissolution rate, $1/\tau$, as a function of inverse temperature, is shown in Figure 9a for the (001) surface at pH 12.9, and in Figure 9b for the (001) and (010) surfaces at pH 1.1. These data are all consistent with Arrhenius behavior—i.e., rate $\sim A \exp(-E_{app}/RT)$, where A is the preexponential factor, and E_{app} is the apparent activation energy—albeit with significantly different slopes that are proportional to the apparent activation energies for dissolution at each pH and for each crystal orientation. At pH 12.9, we find a best-fit apparent activation energy of 65 ± 7 kJ/mol for the (001) surface. At pH 1.1, we find apparent activation energies of 87 ± 7 and 41 ± 7 kJ/mol for the (001) and (010) surfaces, respectively. These measurements reveal apparent activation energies that are significantly different for the (001) surface at acidic and alkaline pH, which is expected based on previous studies. In spite of the high similarity in the nominal structures and dissolution processes for the (001) and (010) surfaces at acidic pH, the apparent activation energies for dissolution of these two surfaces are very different. This difference in apparent activation energies at acidic pH for the (001) and (010) surfaces is unexpected.

4. DISCUSSION

4.1. Comparison with Powder Dissolution Results

Our face-specific dissolution rates and activation energies can be compared directly with powder dissolution results, as both types of measurements quantify the release of material to solution as a function of time. We begin our comparison of the dissolution kinetics at alkaline pH, given the relative simplicity of the dissolution process (i.e., the lack of non-stoichiometry). Although there are few K-feldspar powder dissolution data available at alkaline pH, our derived apparent activation energy for dissolution, 65 ± 7 kJ/mol (Fig. 9a) is consistent with a consensus estimate derived from available powder studies (57.8 kJ/mol; Blum and Stillings, 1995, and references therein). This agreement is especially good, considering that the other data were taken at lower pH values, $9 < pH < 11$. This indicates a reasonable correspondence between the powder and single-crystal dissolution results at alkaline pH.

The dissolution rate as a function of temperature at acidic pH is shown in Figure 9b for the (001) and (010) cleavage surfaces with apparent activation energies of 97 ± 7 and 41 ± 7 kJ/mol, respectively. This is compared to the dissolution rate variation for microcline powder at acidic pH (Schweda, 1989; Blum and Stillings, 1995), which shows an apparent activation energy of 53.6 kJ/mol. (The Schweda [1989] data were measured at pH 3; we scaled the measured rates to account for measured variation of the dissolution rate with pH in powder dissolution measurements, $R \sim 10^{-0.5pH}$ [Blum and Stillings, 1995] so that they could be compared directly with our data.) The apparent activation energies derived from the single-crystal studies therefore bracket the values derived from the powder study. In comparing our data to those of Schweda (1989), we have assumed that the dissolution kinetics of microcline (the phase used in Schweda's experiments) are comparable to those of orthoclase. This is supported by a compilation of results showing an average apparent activation energy for "K-feldspar" dissolution of 51.7 kJ/mol (Blum and Stillings, 1995) that is close to the 53.6 kJ/mol result of Schweda (1989) and is comparable with an average apparent activation energy for albite dissolution at acidic pH of 60 kJ/mol (Blum and Stillings, 1995, and references therein). These single-crystal values are also comparable to activation energies determined for other feldspars, including oligoclase, labradorite, and anorthite (Blum and Stillings, 1995, and references therein). We also find reasonable correspondence between our absolute dissolution rates and those of Schweda, although the single-crystal rates are consistently larger than those derived from steady-state powder measurements at acidic pH (Fig. 9). For example, both single-crystal surfaces have dissolution rates at ~50°C that are 2.4 times larger than the powder results. Yet the single-crystal data in

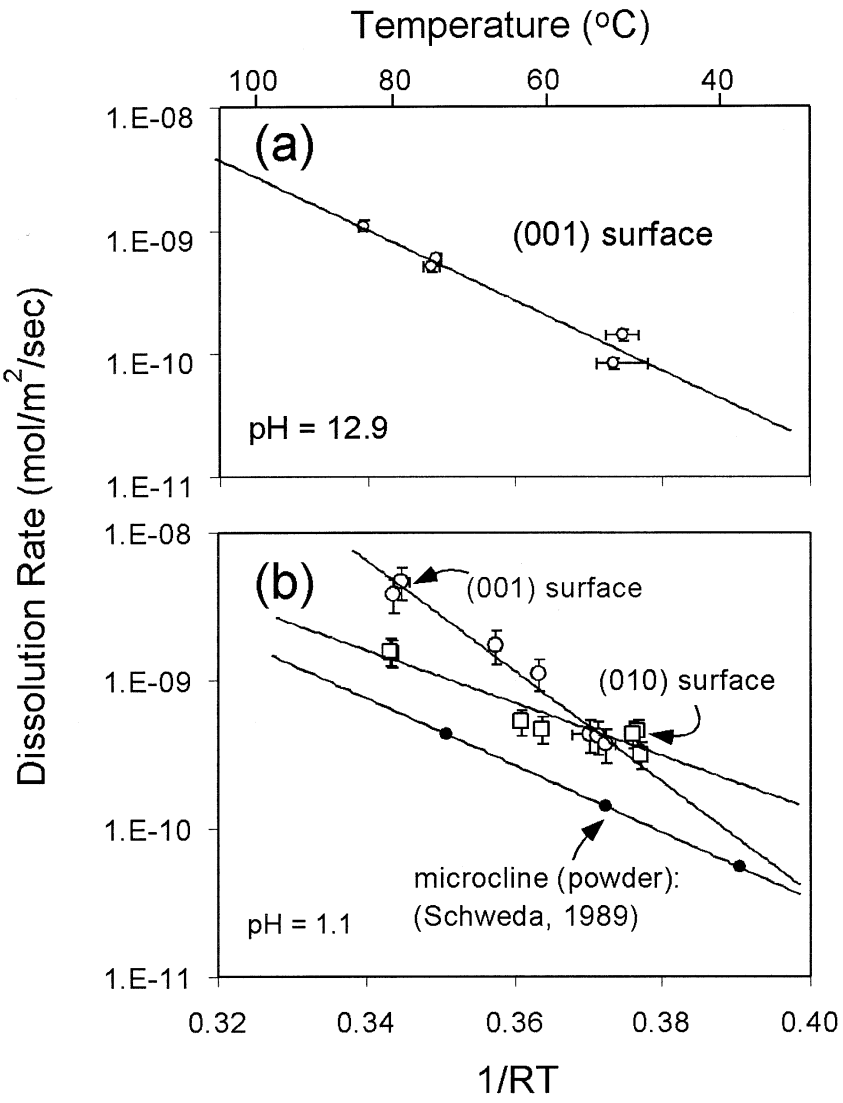

Fig. 9. Plot of measured orthoclase dissolution rates vs. 1/T for (a) the (001) surface at pH 12.9 and (b) the (001) and (010) surfaces at pH 1.1 (shown as open circles and squares, respectively). Also included is a plot of the dissolution rate derived from K-feldspar powder at acidic pH, shown as filled circles (see Schweda, 1989; Blum and Stillings, 1995). The activation energies for the acidic dissolution of orthoclase (001) and (010) surfaces are substantially higher and lower, respectively, than that derived from powder measurements.

Figure 9 are not corrected for the approximate twofold change in dissolution rate that is observed as the single-crystal measurements approach steady state as shown in Figures 7 and 8. Taking this into account, we find only a ~30% difference in absolute dissolution rates at this temperature between the single-crystal and powder results, which is small with respect to the ~10-fold variation in absolute dissolution rates observed in powder measurements between different laboratories (Blum and Stillings, 1995).

The observed anisotropy in face-specific dissolution rates for orthoclase is not associated with any lattice microstructure, as TEM measurements revealed the orthoclase to be homogeneous. Therefore, the observed anisotropy at acidic pH must be an intrinsic property of orthoclase dissolution. The simplest explanation for the difference in the measured activation energies between the (001) and (010) surfaces and that derived from powders is that the apparent activation energy is crystal-face-dependent. The substantially lower apparent activation energy for the (010) surface (with respect to both the (001) surface and powders) is reassuring in that the powder has a heterogeneous distribution of surfaces and the mean apparent activation energy derived from the single-crystal surfaces is close to that of the powder.

An important consideration bearing on the significance of these results is the accuracy and precision of the dissolution rates as measured by X-ray reflectivity. Such measurements yield precise dissolution rates, because the time resolution of the X-ray measurement is small relative to the time constant of the reflectivity changes caused by dissolution. As described previously (Teng et al., 2001), the most precise dissolution rate would be obtained by comparing the dissolution curves in Figures 3, 4, and 6 to an atomistic dissolution model that

quantitatively explains the variation of the reflectivity as a function of time. Because of the many complexities in the dissolution process described above, however, it is not yet sufficiently well understood to derive dissolution rates in this manner. Instead, the relative dissolution rates have been estimated by normalizing the datasets to achieve optimal agreement between dissolution measurements at different temperatures. In this context, high precision can be achieved as long as the dissolution process itself does not change as a function of temperature Operationally, this implies that the shape of the time-normalized dissolution curves, $R[t/\tau(T)]/R(t = 0)$, is invariant with changes in temperature.

We observe excellent consistency in our time-normalized dissolution data at alkaline pH (Fig. 3b) but less consistency for the time-normalized dissolution data at acidic pH (Figs. 4b, 6b). One indication of the accuracy of the measurement is the location of the second intensity maximum in the scaled data (i.e., after normalizing for the differences in dissolution rates). While the alkaline data show little or no variation in the position of the second intensity maximum in the scaled data, the acidic data show a ~20% sample-to-sample variation at the measured temperatures. We can compare this internal systematic error in the dissolution rate to the factor of 12 change in dissolution rate observed at pH 1.1 between 50 and 76°C, and the expected factor of 5 change in dissolution rate based upon the powder dissolution data for the same temperature range (Schweda, 1989; Blum and Stillings, 1995). The estimated 20% error associated with the accuracy of our measurements at acidic pH is substantially smaller than the discrepancy between our data and that derived from powder dissolution measurements.

We previously concluded that dissolution of the orthoclase (001) surface at both acidic and alkaline pH is a balance of two separate molecular-scale processes (i.e., dissolution from terrace and step sites), each of which is represented by individual rate constants, K_d and K_s, respectively (Teng et al., 2001). Assuming that the activation energy for each of these processes is distinct, this implies that it should not be possible, in general, to describe the net dissolution behavior on each surface with a single activation energy, although this might be a reasonable approximation under a limited range of experimental conditions. If the relative variations of the individual dissolution rates as a function of temperature were significant over the measured temperature range, non-Arrhenius behavior (i.e., non-linear dependence of log(Rate) vs. 1/T) should be visible in Figure 9a,b. No such evidence for non-Arrhenius behavior is seen in any of these datasets, although only ~10-fold changes in dissolution rates were probed at each set of conditions so that our sensitivity to non-Arrhenius behavior is limited. While we cannot uniquely establish that only one activation energy is present under our conditions, our data clearly demonstrate that the variation of the dissolution rate on each of these cleavage surfaces at acidic pH is different from that observed with powder samples.

The substantial variation of the apparent activation energy for dissolution as a function of crystallographic orientation at pH 1.1 implies that the anisotropy in dissolution rates is a strong function of temperature. The derived preexponential factors for dissolution of the (001) and (010) surfaces are 3×10^4 and 2×10^{-3}, respectively, and differ by a factor of $\sim 10^7$. This explains why the two surfaces that have different apparent activation energies can also have the same dissolution rate at ~51°C. Thus, while the (001) surface dissolves faster at $T >$ 51°C, the (010) surface is projected to dissolve faster at $T <$ 51°C. There is a ~25-fold change in the ratio of projected dissolution rates for the (001) and (010) surfaces between 25 and 90°C (Fig. 9b). Previous studies of quartz dissolution by AFM found minimal sensitivity to the orientation of the crystal face in the apparent activation energy (Gratz et al., 1990) and found that the face-selected dissolution rates and activation energies were comparable to values derived from bulk powder dissolution measurements (e.g., Dove, 1995). We are only aware of a single study of feldspar dissolution in acidic solutions that explored the anisotropy of dissolution kinetics and activation energies. These macroscopic measurements of thin labradorite disks (cut and polished to size) did not show any clear evidence for anisotropy in either the dissolution rates or activation energies (Suzuki et al., 1996). Because of the many differences in mineral composition and surface preparation, it is not possible to determine if these results reflect intrinsic differences between orthoclase and labradorite. The lack of anisotropy in the labradorite dissolution measurements, however, might be extrinsic. Those surfaces were mechanically polished, which can result in substantial μm-scale surface roughening and near-surface damage that could obscure the anisotropy that we observe on freshly cleaved orthoclase surfaces. In considering other silicate minerals, measurements of fosteritic olivine dissolution found a substantial (~40%) anisotropy in apparent activation energies for three principal crystallographic directions (Awad et al., 2000). These individual apparent activation energies bracketed the activation energy derived from crystallographically averaged measurements.

Our measured apparent activation energies for dissolution of the orthoclase (001) and (010) surfaces at acidic pH bracket the value derived from powder dissolution measurements for K-feldspar. If these two cleavage surfaces were the dominant surfaces expressed by powders, the present single-crystal results would imply that a plot of log(rate) vs. 1/T for the powder would be non-linear over this temperature range. However, the powder dissolution data show no evidence for any such non-Arrhenius behavior. In the case of orthoclase dissolution (and possibly for other feldspars as well), the range of surface orientations and the variable distribution of defects inherent to powder dissolution measurements may produce an apparent activation energy that is neither simply the average of the activation energies of exposed crystal faces nor representative of a single fundamental process. Many complexities associated with the powder dissolution measurements are eliminated by using single-crystal cleavage planes for such measurements.

4.2. Dissolution Anisotropy at pH 1.1

The orthoclase (001) and (010) surfaces have similar structures. Each surface exposes a different side of the same tetrahedral ring; the cleavage plane is coincident with the plane in which the potassium atoms reside in the bulk lattice—this assumption has been directly confirmed for the (001) surface (Fenter et al., 2000)—and the (001) and (020) plane spacings are nearly identical (6.459 vs. 6.503 Å, respectively), as are the unit cell areas per tetrahedral ring (55.8 vs. 55.4 Å^2, respec-

tively). Each of these cleavage surfaces exposes two crystallographically distinct tetrahedral sites: the T1 and T2 sites. In each case, one of these sites is terminated with a non-bridging oxygen (NBO) due to cleavage, while the other is fully coordinated by bridging oxygen sites. The main difference between these two cleavage surfaces is that the T1 site is terminated with an NBO on the (001) surface, while the T2 site is terminated with an NBO on the (010) surface. This difference may be significant, since the Al occupancies for these two sites are different. The Al occupation is 0.352 in the T1 site and 0.148 in the T2 site (with corresponding Si occupancies of 0.648 and 0.852, respectively) (Kimata et al., 1996).

The Al tetrahedral site is generally believed to be the primary reactive site at acidic pH (Kubicki et al., 1996), and our previous measurements on the (001) surface provide independent support that Al is preferentially depleted in the outermost unit cell, at least during the initial phase of dissolution (Teng et al., 2001). The number of Al sites that are exposed by the (001) and (010) cleavage surfaces is the same, but the distribution of these Al sites between the T1 and T2 sites is different, so that the number of Al sites having an NBO for each surface will be different. This indicates that the different dissolution behavior for the two surfaces may be associated with the incomplete ordering of Al in the orthoclase lattice. However, the differences in activation energies and preexponential factors for the (001) and (010) surfaces, and especially the crossover of the kinetically preferred surface for dissolution at 51°C, at first appears difficult to reconcile based solely on the related differences in the fraction of Al sites having an NBO (which differs by only a factor of ~2.4 for these surfaces).

It is well established that the apparent activation energy for mineral dissolution can exhibit substantial variation as a function of pH for otherwise similar solution conditions and that these changes are typically coupled with orders of magnitude changes in the preexponential factor (Carroll and Walther, 1990; Casey and Sposito, 1992; Casey et al., 1993). In two well-documented systems (tephroite and kaolinite), the activation energies appear to be correlated with the logarithm of the preexponential factors, such that a reduction in the apparent activation energy by a factor of ~2 to 3 is coupled with a reduction of preexponential factors by 10 to 12 orders of magnitude. Our observation of a twofold difference in apparent activation energies, coupled with a $\sim 10^7$-fold difference in preexponential factors for the (001) and (010) surfaces, indicates that the different dissolution behavior of the (001) and (010) surfaces is real and may have the same origin as the pH-dependence of apparent activation energies. There are two theoretical frameworks that have been used to explain the pH dependence of the apparent activation energies (Casey and Sposito, 1992; Lasaga et al., 1994). We discuss the general characteristics of each formalism in relation to our present observations.

Casey and Sposito (1992) showed that the apparent activation energy for proton-promoted dissolution, E_{exp}, can depend on not only the temperature variation of the intrinsic rate constant, $\partial(\ln k')/\partial(1/T)$, but also on changes in the pH through the associated changes in protonated reactive site density through the relation:

$$E_{exp} = -R[\partial(\ln k')/\partial(1/T)] - n(1 - X_{SOH2+})(\Delta H(int) - F\psi_S) \quad (1)$$

where the dissolution rate is assumed to vary as $R_{dis} = k' x^n_{SOH2+}$, where k' is a rate constant, x_{SOH2+} is the fraction of reactive sites that are protonated, n is the partial reaction rate order, ΔH(int) is a proton desorption enthalpy, ψ_s is the surface potential, and F is the Faraday constant. Within this context, the rates derived in Figure 9a,b are not intrinsic rates (i.e., per reactive site). Instead, they are averaged over the macroscopic surface areas over which the site density of reactive sites may change with solution conditions. An important prediction of this model is that the apparent activation energy derived from dissolution experiments is expected to depend on the solution conditions (i.e., pH) due to changes in the protonation of reactive sites. The activation energy is linearly proportional to changes in the second term on the right-hand side of Eqn. 1. Thus, substantial changes in the reactive site density, fraction of reactive sites, the proton desorption enthalpy, or the surface potential for these two surfaces could, in principle, be the cause of the anisotropy observed in Figure 9b. Given the crystallographic similarity of these two surfaces, the anisotropy in apparent activation energies might be reasonably attributed to the different densities of Al sites having an NBO (i.e., aluminol sites) for the (001) and (010) surfaces, because that appears to be the main difference between the two surfaces. In particular, the 2.4-fold difference in apparent activation energies is, within error, identical to the ratio of aluminol site densities for the two surfaces, and the surface with the larger aluminol site density is the surface with the larger apparent activation energy. Even if this formalism is ultimately determined to be the main contribution to the anisotropy in apparent activation energies, we expect this one-to-one correspondence to be fortuitous, since the apparent activation energy is a sum of at least two terms, and a one-to-one correspondence would suggest that the first term in Eqn. 1 is negligible in magnitude.

There are, however, a number of additional issues that must be considered. First, this relation was derived for the simpler case of oxide dissolution. Although it has also been applied to dissolution of silicates (Casey et al., 1993), some of the assumptions that were used to derive this relation may be too simple to properly represent the more complex dissolution process for feldspars, especially with respect to inclusion of differential site reactivity (e.g., of aluminol and silanol sites) and the possible non-stoichiometry of dissolution at acidic pH. Second, recent systematic measurements have shown that the apparent activation energy of albite powder dissolution at acidic pH is independent of pH (Chen and Brantley, 1997). This lack of pH dependence of the activation energy for albite dissolution suggests, at face value, that the contribution of the second term in Eqn. 1 is insignificant for albite (and by inference, K-feldspars as well), at least for the powder dissolution data. The present data, in contrast, demonstrate a strong anisotropy in activation energies. We must consider the possibility that any pH dependence of the activation energy derived from powder dissolution might have been obscured by the crystallographic anisotropy of the activation energy, especially given the potentially wide and inhomogeneous distribution of cleav-

age faces and fracture surfaces that are intrinsic to powder dissolution measurements.

A separate theoretical approach that has been used to explain the variation of the apparent activation energy as a function of pH is based on the deviation from equilibrium effect (Lasaga et al., 1994; Cama et al., 1999). Here, the dissolution rate is assumed to vary with the free energy of the dissolution reaction, ΔG, and is assumed to be proportional to a factor, $f(\Delta G)$, where $f(\Delta G) = 1$ far from equilibrium and $f(\Delta G) = 0$ at equilibrium. Transition-state theory predicts that $f(\Delta G) = -[1 - \exp(\Delta G/RT)]$ (Aagaard and Helgeson, 1982), which implies that the dissolution rate will be insensitive to ΔG for sufficiently large values (i.e., $\Delta G \ll -RT$), resulting in a "dissolution plateau." The upper limit of ΔG in the plateau regime depends strongly on the mineral; values for various silicate minerals include $\Delta G < -3$ kJ/mol for gibbsite (at pH 3, 80°C) (Nagy and Lasaga, 1992), < -8 kJ/mol for kaolinite (at pH 3, 80°C) (Nagy and Lasaga, 1993), and < -38 kJ/mole for albite (at pH 8.8, 80°C) (Burch et al., 1994). This formalism has been used to explain the strong variation of apparent activation energies of kaolinite (Cama et al., 1999). This approach does not appear to explain the present findings. First, it is not immediately apparent how this formalism would translate into a substantial difference in apparent activation energies for two similar crystal faces of the same mineral under otherwise identical experimental conditions. Second, we have calculated ΔG for orthoclase dissolution at pH 1.1 at temperatures ranging from 78 to 46°C and find $\Delta G = -163$ and -198 kJ/mol at the upper and lower temperature extremes, respectively. While we are unaware of any measurements of $f(\Delta G)$ for albite or orthoclase at acidic pH, these large free-energy differences are substantially more negative than the values quoted above for gibbsite, kaolinite, and albite. This suggests that we are well within the dissolution plateau regime, and, therefore, the dissolution rates should be independent of ΔG. Third, we note that a separate measure of the sensitivity of the dissolution kinetics to ΔG is the ratio of fluid flux to reactive surface area, q/A. The present measurements were performed with single-crystal surfaces having q/A $\sim$ (3 mL/h)/($\sim$30 mm^2) $\approx$ 1500 mL/m^2/min, whereas a typical value for powder dissolution measurements is q/A = 0.002 mL/m^2/min (Cama et al., 1999), and the importance of the far-from-equilibrium effect becomes larger as the value of q/A becomes smaller. The $\sim 10^6$-fold larger value of q/A indicates, therefore, that the present measurements were performed in a regime in which the sensitivity of kinetics to changes in ΔG were negligible.

We conclude that the present results cannot be explained simply by differences in the value of ΔG for dissolution of the two surfaces. It is not yet possible to be definitive as to whether this anisotropy can be understood solely or even primarily within the context of a proton-promoted dissolution mechanism (Casey and Sposito, 1992). The results are, however, consistent with a proton-mediated dissolution mechanism, especially given the unexpected correspondence between the apparent activation energy and the aluminol site densities of these two surfaces. Additional X-ray reflectivity measurements can test the applicability of Eqn. 1 as a basis to understand the observed anisotropy in dissolution kinetics at pH 1.1.

4.3. Applicability of X-ray Reflectivity as a Probe of Mineral Dissolution

The primary limitation of X-ray reflectivity for probing mineral dissolution rates is the time that is needed to measure the reflectivity signal (in the presence of an incoherent background) as compared with the time for dissolving a single layer. Most of these measurements were performed at the BESSRC 12-BM bending magnet beamline that has a typical flux of $\sim 3 \times 10^{10}$ photons/s at an energy of $\sim$19.5 keV. A flux of $\sim 2 \times 10^9$ photons/s is obtained when the vertical beam size is reduced to 0.1 mm (to avoid spill-off from the $\sim$4-mm-long sample at an incident angle of $\sim$1.5°). The transmission of our cell at 19.5 keV is 0.73 due to linear attenuation through the solution and Kapton windows. Finally, the reflectivity at the first anti-Bragg condition is $\sim 10^{-6}$ for a freshly cleaved orthoclase (001) surface (Fenter et al., 2000). A specular reflection signal of $\sim 10^3$ photons/s from a freshly cleaved surface can be measured under these conditions (as shown in Fig. 1c) with a typical background count rate of $\sim$40 counts per second. Given that the first intensity minimum during a typical dissolution experiment at acidic pH is $\sim 100\times$ weaker than the initial reflectivity, it is necessary to measure a reflectivity signal of $\sim$10 photons/s superimposed over a background of 40 photons/s. To measure the reflectivity with a statistical uncertainty of $\sim$20% near the reflectivity minima then requires $\sim$25 s of counting time per point in the rocking curve, or $\sim$10 min per rocking curve. If we measure the reflectivity at equal intervals, the time to remove a single layer should be $\sim 10\times$ longer than the time to perform a single scan. Measurement rates as high as 0.6 layer/h, or 10^{-9} mol/m^2/s, can be achieved under these conditions. Measurements at alkaline pH can be performed for faster dissolution rates, because the reflectivity is never observed to decrease by more than a factor of 10 during dissolution at alkaline pH; this is reflected in the substantially smaller error bars on each data point at alkaline pH as compared with acidic pH.

The maximum dissolution rate measurable by X-ray reflectivity could be substantially increased by measuring the rocking-curve data using a linear detector that simultaneously records the entire rocking-curve scan (resulting in a $\sim$20-fold decrease in measurement time), or by using brighter sources such as undulators having $\sim 100\times$ higher photon flux under similar conditions. Together, such improvements would further increase the upper range of dissolution rates by a factor of $\sim$1000, so that dissolution rates as high as $\sim$1000 layer/h (or $\sim 10^{-6}$ mol/m^2/s) could thus be measured. At the other extreme, the ability to measure slow dissolution rates is limited by the practical length of a given synchrotron experiment ($\sim$1 week), putting a lower limit at $\sim$1 layer/d or $\sim 10^{-12}$ mol/m^2/s. Dissolution rates can be measured over the range, $\sim 10^{-12}$ to 10^{-6} mol/m^2/s. This range of dissolution rates accessible to X-ray reflectivity measurements encompasses all dissolution rates reported for alkali feldspars, as reviewed by Blum and Stillings (1995), with the exception of the slowest dissolution rates near neutral pH.

A more fundamental limit to the type of systems that can be studied in this manner is the character of the dissolution process. Orthoclase dissolution is ideal for probing with X-ray reflectivity, because the only microtopographical inhomogene-

ity that is observed during dissolution (e.g., the formation of nanometer-sized pores at acidic pH) is well within the resolution of the X-ray reflectivity measurement. Otherwise, the mineral dissolves uniformly over the μm-sized coherence length of the X-ray beam. Systems having a stronger tendency to roughen during dissolution would be more difficult to study. The relatively rapid roughening in the present results at acidic pH was challenging to measure because of the loss of reflected intensity.

A separate limitation of this approach is that the dissolution rate is determined by the period of the reflectivity oscillations as seen in Figure 2. The observation of oscillations requires that there be two types of reactive sites (e.g., terrace and step sites). For instance, a mineral that reacts only by a terrace dissolution process without a separate step dissolution produces an exponentially decreasing reflectivity without oscillations (Teng et al., 2001), where the time constant of the exponential fall-off is proportional to the dissolution rate, K_d. However, this approach would likely be a less accurate measure of the dissolution rate, as it could be subject to numerous sources of systematic error. Conversely, minerals that dissolve purely by step motion produce negligible changes in reflectivity during dissolution.

5. CONCLUSION

We have demonstrated the use of X-ray reflectivity as a probe of mineral dissolution kinetics through real-time measurements of the reflectivity at the anti-Bragg condition. Direct measurements of the dissolution kinetics as a function of temperature were presented for the (001) surface at pH 12.9 and for the orthoclase (001) and (010) surfaces at pH 1.1. These data provide precise determinations of the face-specific apparent activation energy associated with orthoclase dissolution. The activation energy derived here at pH 12.9 for the (001) surface, 65 ± 7 kJ/mol, is in reasonable agreement with powder dissolution measurements at alkaline pH. Measured activation energies for the (001) and (010) cleavage surfaces at pH 1.1, 87 ± 7 and 41 ± 7 kJ/mol, respectively, are substantially different from results derived from powder dissolution measurements at acidic pH. This indicates that the kinetics and energetics of dissolution depend in a non-trivial way on the mineral face on which dissolution occurs and suggests that the activation energies derived from powder measurements may not typically reflect a single dissolution mechanism.

In summary, we can make the following general observations:

1. The substantial differences in the dissolution behavior of the (001) and (010) surfaces at acidic pH, coupled with their similarity in structure and composition (e.g., having similar surface compositions and distributions of reactive sites), reinforces previous observations (Teng et al., 2001) that the dissolution behavior cannot be understood solely on the chemical nature of individual sites. This would change the dissolution rates only by modest factors for the (001) and (010) surfaces and would not explain the large differences in activation energies or preexponential factors. Instead, we expect that it will be necessary to develop a more complete understanding of the reactive surface, including an explicit description of the spatial distribution of reactive sites (e.g., terrace sites vs. step sites).
2. We must still determine if the differences in dissolution kinetics are related to any structural difference between the (001) and (010) surfaces. The structure of the (001) surface has been determined (Fenter et al., 2000), revealing that the surface tetrahedral sites are fully coordinated through adsorption of an oxygen-containing species (e.g., OH). While it is likely that the structure of the (010) surface will be similar in detail, measurements of the (010) surface structure and termination are in progress and will ultimately help to determine if the difference in reactivity of the (010) and (001) surfaces is related to any difference in the structure of these surfaces.
3. The similar ratio of activation energies and aluminol site densities between the (001) and (010) surfaces suggests that the ultimate cause may be described within the context of the theory by Casey and Sposito (1992). Based on the limited data presented here, however, it is not possible to definitely determine if this theory can uniquely explain the large anisotropy in activation energies observed at pH 1.1.
4. The initial dissolution rates at acidic pH for freshly cleaved single-crystal surfaces are found to be within a factor of 2 of the longer-term rates as measured on these single-crystal surfaces and appear to reach the steady-state value upon dissolution of three layers. This transient variation of the dissolution rate is smaller than that observed in powder dissolution studies. This indicates that the transient initial rates of powder dissolution measurements for $T < 100$°C derive largely from extrinsic characteristics (sample preparation, surface damage) as opposed to the intrinsic reactivity of alkali feldspars.

Acknowledgments—This work was supported by the Geosciences Research Program, Office of Basic Energy Sciences, Office of Science, U.S. Department of Energy under contract W-31-109-Eng-38. Measurements were performed at the BESSRC sector of the APS, beamlines 12-ID-D, 11-ID-D, and 12-BM-B. Use of the Advanced Photon Source also was supported by the Office of Basic Energy Sciences. We thank Roland Hellmann, K. L. Nagy, and two anonymous reviewers for comments that helped substantially to improve this manuscript.

Associate editor: D. Wesolowski

REFERENCES

Aagaard P. and Helgeson H. C. (1982) Thermodynamics and kinetic constraints on reaction rates among minerals and aqueous solutions. I. Theoretical considerations. *Am. J. Sci.* **282,** 237–285.

Awad A., Koster van Groos A. F., and Guggenheim S. (2000) Forsteritic olivine: Effect of crystallographic direction on dissolution kinetics. *Geochim. Cosmochim. Acta* **64,** 1765–1772.

Bevington P. R. (1969) *Data Reduction and Error Analysis for the Physical Sciences*. MacGraw-Hill Book Company, New York.

Blum A. E. and Stillings L. L. (1995) Feldspar dissolution kinetics. In *Chemical Weathering Rates of Silicate Minerals* (ed. A. F. White and S. L. Brantley). *Rev. Mineral.* **31,** 291-351.

Bosbach D. and Rammensee W. (1994) In situ investigation of growth and dissolution on the (010) surface of gypsum by scanning force microscopy. *Geochim. Cosmochim. Acta* **58,** 843–849.

Brantley S. L. and Stillings L. L. (1997) Reply to comment: Feldspar dissolution at 25°C and low pH. *Am. J. Sci.* **297,** 1021–1032.

Burch T. E., Nagy K. L., and Lasaga A. C. (1994) Free energy dependence of albite dissolution kinetics at 80C, pH 8.8. *Chem. Geol.* **105,** 137–162.

Cama J., Ayora C., and Lasaga A. C. (1999) The deviation from equilibrium effect on dissolution rate and apparent variations in activation energy. *Geochim. Cosmochim. Acta* **63,** 2481–2486.

Carroll S. A. and Walther J. V. (1990) Kaolinite dissolution at 25, 60 and 80°C. *Am. J. Sci.* **290,** 797–810.

Casey W. H. and Sposito G. (1992) On the temperature dependence of mineral dissolution rates. *Geochim. Cosmochim. Acta* **56,** 3825–3830.

Casey W. H., Westrich H. R., Massis T., Banfield J. F., and Arnold G. W. (1989) The surface chemistry of labradorite feldspar after acid hydrolysis. *Chem. Geol.* **78,** 205–218.

Casey W. H., Hochella M. F. Jr., and Westrich H. R. (1993) The surface chemistry of magnaniferous silicate minerals as inferred from experiments on tephriote (Mn_2SiO_4). *Geochim. Cosmochim Acta* **57,** 785–793.

Chen Y. and Brantley S. L. (1997) Temperature- and pH-dependence of albite dissolution rate at acid pH. *Chem. Geol.* **135,** 275–290.

Chen Y., Brantley S. L., and Ilton E. S. (2000) X-ray photoelectron spectroscopic measurement of the temperature dependence of leaching of cations from the albite surface. *Chem. Geol.* **163,** 115–128.

Chou L. and Wollast R. (1984) Study of the weathering of albite at room temperature and pressure with a fluidized bed reactor. *Geochim. Cosmochim. Acta* **48,** 2205–2218.

Dove P. M. (1995) Kinetic and thermodynamic controls on silica reactivity in weathering environments. In *Chemical Weathering Rates of Silicate Minerals* (ed. A. F. White and S. L. Brantley)., *Rev. Mineral.* **31,** 235-290.

Dove P. M. and Platt F. M. (1996) Compatible real-time rates of mineral dissolution by atomic force microscopy. *Chem. Geol.* **127,** 331–338.

Feidenhans'l R. (1989) Surface structure determination by X-ray diffraction. *Surf. Sci. Rep.* **10,** 105–188.

Fenter P., Teng H., Geissbühler P., Hanchar J. M., Nagy K., and Sturchio N. C. (2000) Atomic-scale structure of the orthoclase (001)-water interface measured with high-resolution X-ray reflectivity. *Geochim. Cosmochim. Acta* **64,** 3663–3673.

Gout R., Oelkers E. J., Schott J., and Zwick A. (1997) The surface chemistry and structure of acid-leached albite: New insights on the dissolution mechanism of the alkali feldspars. *Geochim. Cosmochim. Acta* **61,** 3013–3018.

Gratz A. J., Bird P., and Quiro G. B. (1990) Dissolution of quartz in aqueous basic solution, 106–236°C: Surface kinetics of "perfect-crystallogographic faces. *Geochim. Cosmochim. Acta* **54,** 2911–2922.

Gratz A. J., Manne S., and Hansma P. K. (1991) Atomic force microscopy of atomic-scale ledges and etch pits formed during dissolution of quartz. *Science* **251,** 1343–1346.

Hellmann R. (1994) The albite-water system: Part I. The kinetics of dissolution as a function of pH at 100, 200 and 300°C. *Geochim. Cosmochim. Acta* **58,** 595–611.

Hellmann R. (1995) The albite-water system: Part II. The time evolution of the stoichiometry of dissolution as a function of pH at 100, 200, and 300 °C. *Geochim. Cosmochim. Acta* **58,** 595–611.

Hellmann R., Eggleston C. M., Hochella M. F. Jr., and Crerar D. A. (1990) The formation of leached layers on albite surfaces during dissolution under hydrothermal conditions. *Geochim. Cosmochim. Acta* **54,** 1267–1281.

Hellmann R., Dran J. C., and Della Mea G. (1997) The albite-water system: Part III. Characterization of leached and hydrogen-enriched layers formed at 300°C using MeV ion beam techniques. *Geochim. Cosmochim. Acta* **61,** 1575–1594.

Higgins S. R., Eggleston C. M., Jordan G., Knauss K. G., and Boro C. O. (1998) In-situ observation of oxide and silicate mineral dissolution by hydrothermal scanning force microscopy: Initial results for hematite and albite. *Mineral. Mag.* **62A,** 618–619.

Hillner P. E., Gratz A. J., Manne S., and Hansma P. K. (1992) Atomic scale imaging of calcite growth and dissolution in real time. *Geology* **20,** 359–362.

Holdren G. R. Jr. and Speyer P. M. (1985) pH-dependent changes in the rates and stoichiometry of dissolution of an alkali feldspar at room temperature. *Am. J. Sci.* **285,** 994–1026.

Inskeep N. P., Nater E. A., Bloom P. R., Vandervort D. S., and Erich M. S. (1991) Characterization of laboratory weathered labradorite surfaces using X-ray photoelectron spectroscopy and transmission electron microscopy. *Geochim. Cosmochim. Acta* **55,** 787–800.

Jordan G. and Rammensee W. (1998) Dissolution rates of calcite (104) obtained by scanning force microscopy: Microtopography-based dissolution kinetics on surfaces with anisotropic step velocities. *Geochim. Cosmochim. Acta* **62,** 941–947.

Jordan G., Higgins S. R., Eggleston C. M., Swapp S. M., Janney D. E., and Knauss K. G. (1999) Acidic dissolution of plagioclase: In situ observations by hydrothermal atomic force microscopy. *Geochim. Cosmochim. Acta* **63,** 3183–3191.

Kimata M., Saito S., Shimizu M., Iida I., and Tomoaki M. (1996) Low-temperature crystal structures of orthoclase and sanidine. *Neues Jb. Miner. Abh.* **171,** 199–213.

Kubicki J. D., Blake G. A., and Apitz S. E. (1996) Ab initio calculations on aluminosilicate Q^3 species: Implications for atomic structures of mineral surfaces and dissolution mechanisms of feldspars. *Am. Mineral.* **81,** 789–799.

Lasaga A. C., Soler J. M., Ganor J., Burch T. E., and Nagy K. L. (1994) Chemical weathering rate laws and global geochemical cycles. *Geochim Cosmochim. Acta* **58,** 2361–2386.

Liang Y. and Baer D. R. (1997) Anisotropic dissolution at the CaCO3(1014)-water interface. *Surf. Sci.* **373,** 275–287.

Liang Y., Baer D. R., McCoy J. M., Amonette J. E., and LaFemina J. P. (1996) Dissolution kinetics at the calcite-water interface. *Geochim. Cosmochim. Acta* **60,** 4883–4887.

Muir I. J., Bancroft F. M., and Nesbitt H. W. (1989) Characteristics of altered labradorite surfaces by SIMS and XPS. *Geochim. Cosmochim. Acta* **53,** 1235–1241.

Nagy K. L. and Lasaga A. C. (1992) Dissolution and precipitation kinetics of gibbsite at 80C and pH 3. The dependence on solution saturation state. *Geochim. Cosmochim. Acta* **56,** 3093–3111.

Nagy K. L. and Lasaga A. C. (1993) Simultaneous precipitation kinetics of kaolinite and gibbsite at 80C and pH 3. *Geochim. Cosmochim. Acta* **57,** 4329–4335.

Nugent M. A., Brantley S. L., Pantano C. G., and Maurice P. A. (1998) The influence of natural mineral coatings on feldspar weathering. *Nature* **395,** 588–591.

Petrovic R. (1976) Rate control in dissolution of alkali feldspars: I. Study of residual feldspar grains by X-ray photoelectron spectroscopy. *Geochim. Cosmochim. Acta.* **40,** 537–548.

Robinson I. K. (1986) Crystal truncation rods and surface roughness. *Phys. Rev. B* **33,** 3830–3836.

Robinson I. K. and Tweet D. J. (1992) Surface X-ray diffraction. *Rep. Prog. Phys.* **55,** 599–651.

Schweda P. (1989) Kinetics of alkali feldspar dissolution at low temperature. In *Proc. 6th Int. Symp. of Water-Rock Interaction* (ed. D. L. Miles), pp. 609–612, Balkema, Rotterdam.

Shiraki R., Rock P. A., and Casey W. H. (2000) Dissolution kinetics of calcite in 0.1 M NaCl solution at room temperature: An atomic force microscopy study. *Aquat. Geochem.* **6,** 87–108.

Stillings L. L. and Brantley S. L. (1995) Feldspar dissolution at 25°C and pH 3: Reaction stoichiometry and the effect of cations. *Geochim. Cosmochim. Acta* **59,** 1483–1496.

Suzuki M., Tokuhei T., Takeshi H., and Tsukimura K. (1996) Dissolution process and rate in feldspar: Effects of crystallographic orientation. *Mineral. J.* **18,** 43–53.

Teng H., Fenter P., Cheng L., Sturchio N. C. (2001) Resolving orthoclase dissolution processes with atomic force. Microscopy and X-ray reflectivity. *Geochim. Cosmochim. Acta* **65**(20), 3459–3474.

van der Vegt H. A., van Pinxteren H. M., Lohmeier M., Vlieg E., and Thornton J. M. C. (1992) Surfactant-induced layer-by-layer growth of Ag on Ag(111). *Phys. Rev. Lett.* **68,** 3335–3338.

Walther J. V. (1997) Comment: Feldspar dissolution at 25 degrees C and low pH. *Am. J. Sci.* **297,** 1012–1021.